# Supplementary Information

# Thermodynamic and kinetic behavior of glycerol aerosol

Timothy P. Wright[1], Chen Song[2], Stephen Sears[2], Markus D. Petters[1]

[1]Department of Marine, Earth, and Atmospheric Sciences, North Carolina State University, Raleigh, NC 27695
[2]RJ Reynolds Tobacco, Winston-Salem, NC 27101

*Corresponding author: M. D. Petters

Contents:

1. Differential mobility analyzer (DMA) equations
2. Mass transfer equations
3. Values and parameterizations used in this work
4. Evaporation in DMA
5. Hygroscopic growth parameterization
6. Measured humidigrams

## Introduction

This supplemental information document provides additional equations, parameters, and values needed to solve Eqs. (1) in the main document. In addition there is discussion in regards to vapor buildup within the differential mobility analyzer and a summary of the equilibrium hygroscopic growth parameterization for glycerol (GLY) and propylene glycol (PG). The document ends with the raw humidigrams used to generate Figure 8 in the main text.

**SI Section 1: Differential mobility analyzer (DMA) equations**

To determine the voltage that will allow for a particle with a changing electrical mobility to transit the DMA, the position of the particle needs to be tracked. The following equations apply to a column type DMA. Particle transit through the DMA is split in two components, radial ($r$) and axial ($z$). Radial motion is forced by the electric field while streamwise motion is forced by the flow field. Particle motion within the DMA is governed by the following equations.

$$\frac{dr}{dt} = Z_p\left(D_p\right)E_r(V) = \frac{eC_c}{3\pi\nu_a D_p}\frac{V}{r ln(r_2/r_1)} \quad \text{(SI 1.1)}$$

where $V$ is the voltage, $r_1$ and $r_2$ are the radial dimensions of the column wall and center electrode, respectively, $e$ is the elementary charge, $C_c$ is the Cunningham correction factor, and $\nu_a$ is the gas viscosity (Knutson and Whitby, 1975).

Movement in the axial or streamwise direction ($z$) was found by treating the particle as a passive tracer within the sheath flow. As derived in Wilkes (2005; see Ch 6.5, Eq. E6.5.8), a steady, incompressible, laminar flow of a Newtonian fluid in an infinitely long round pipe annulus of inner radius $r_1$ and outer radius $r_2$, the expression for the velocity field in the annular space in the pipe is:

$$u_z = \frac{1}{4\mu}\left(-\frac{\partial P}{\partial z}\right)\left[\frac{\ln(r/r_1)}{\ln(r_2/r_1)}(r_2^2 - r_1^2) - (r^2 - r_1^2)\right] \quad \text{(SI 1.2)}$$

Ignoring gravity and assuming a constant pressure gradient of $dP/dz$, Eq. SI 1.2 can be integrated to get the volume flow rate:

$$\frac{dz}{dt} = u_z(r) = \frac{A_1}{A_2}, \quad \text{(SI 1.3)}$$

$$A_1 = \frac{-2Q_s ln(r_2/r_1)\left(r^2 + r_1^2 ln(r/r_2) - r_2^2 ln(r/r_1)\right)}{ln(r/r_2)}$$

$$A_2 = \pi(2ln(r_1/r_2)r_1^4 + ln(r_2/r_1)r_1^4 + ln(r_2/r_1)r_2^4 - r_1^4 + 2r_1^2 r_2^2 - r_2^4)$$

where $Q_s$ is the DMA sheath flow rate.

**SI Section 2: Particle mass transfer equations**

The functional form of the mass transfer rate of a particle composed of *i* species is (Xue et al., 2005):

$$\frac{dm_i}{dt} = \frac{2\pi D_p D_i MW_i \beta(Kn,\alpha_m)}{R}\left(\frac{p_{i,\infty}}{T_\infty} - \frac{p_i}{T}\right), \quad \text{(SI 2.1)}$$

where $m_i$ is the mass of the *i*-th component, $D_p$ is the total particle diameter, $D_i$ is the binary diffusion constant for species *i* in air, $MW_i$ is the molecular weight, $\beta\left(Kn, \alpha_{m,i}\right)$ is the Fuchs mass flux correction term, $Kn = 2\,\lambda_i/D_p$ is the Knudsen number, $\lambda_i$ is mean free path of a gas phase molecule of species *i* in air (evaluated using the kinetic theory of gases: $\lambda = 3\,D_i/[(8\,RT/\pi MW)]^{1/2}$), $\alpha_m$ is mass accommodation coefficient corresponding to the ratio of molecules that collide and stick with the particle to the total number of molecules that collide with the particle, $R$ is the universal gas constant, $p_{i,\infty}$ and $p_i$ are the ambient partial pressure and equilibrium vapor pressure over the droplet surface, respectively, and $T_\infty$ and $T$ are the ambient and particle temperature, respectively. Note that Eq. 1c can be derived from Eq. SI 2.1 when the material dependent parameter is defined such that: $\mu_i = \frac{12}{RT}\frac{D_i MW_i}{\rho_i}$, where $\rho_i$ is the density of the *i*th species.

The Fuchs correction term is a unitless correction term that is applied to the mass transfer equation to modify the mass flux terms when the particle is in the transition regime (Fuchs and Sutugin, 1971). Several functional forms for evaluating this correction term are summarized in Table 1 of Xue et al. (2005) and application of these yielded minimal changes in the modeling results. We selected the correction term from Fuchs and Sutugin (1971).

$$\beta(Kn, \alpha_m) = \frac{1+Kn}{1+0.3773Kn+1.33Kn(1+Kn)/\alpha_m} \quad \text{(SI 2.2)}$$

Here, it is assumed that latent heat is negligible and that the particle system has reached temperature equilibrium with the surrounding gas so that $T_\infty = T$. The saturation ratio of species *i* is defined as $S_i = p_i/p_{i,sat}$. For water vapor, $S \times 100$ corresponds to the relative humidity (RH) of air expressed as percentage. In a dry environment, $S_i = 0$ and thus $p_{i,\infty} = 0$.

The equilibrium vapor pressure over a curved drop surface is enhanced relative to that of over a flat surface

$$p_i = \gamma_i p_{i,sat} exp\left(\frac{4\sigma_i MW_i}{D_p \rho_i RT}\right), \quad \text{(SI 2.3)}$$

where $\sigma_i$ is the surface tension or surface free energy, $\rho_i$ is the density, and $\gamma_i$ is the activity coefficient.

Activity coefficients were obtained from bulk solution data and parameterized using the Margules model (Prausnitz et al., 1999):

$$ln\gamma = \alpha_m(1 - x_w)^{\beta_m}, \quad \text{(SI 2.4)}$$

where $\alpha_m$ and $\beta_m$ are empirical fit parameters and $x_w$ is the mole fraction of water in solution.

Diffusivity of the component particle molecules into the surrounding gas is dependent on component material and surrounding gas parameters and temperature. Diffusivity is estimated from Bird et al. (2002; Eq. 17.3-12),

$$D_i = \frac{0.0018583}{p\,\sigma^2\Omega_D}\sqrt{T^3\left(\frac{1}{MW_i} + \frac{1}{MW_{air}}\right)}. \quad \text{(SI 2.5)}$$

Here $p$ is pressure in atmospheres, σ is the collision diameter, $\Omega_D$, is the collision integral, and $MW_i$ and $MW_{air}$ are the average molecular weight of species $i$ and air, respectively. The collision diameter is calculated from $\sigma = 1/2\,(\sigma_A + \sigma_B)$ (Bird et al., 2002; Bilde et al., 2003), where $\sigma_A$ is the collision diameter of a molecule of the particle and $\sigma_B$ is the collision diameter of the surrounding gas. In the absence of experimental data for the collision diameter, $\sigma_A$ can be estimated from the critical volume, $V_c$, which in turn can be estimated using the Lyderson group contribution method (Lyderson, 1955; Bird et al., 2002; Bilde et al., 2003): $\sigma_A = 0.841V_c^{1/3}$. The collision integral, $\Omega_D$, is found by first determining the critical temperature, $T^* = T/(\epsilon/k_B)$, where the denominator is a Lennard-Jones parameter and is evaluated as $\epsilon/k_B = \sqrt{\epsilon_A\epsilon_B/k_B^2}$. Here, $\epsilon_B/k_B$ is the parameter for the surrounding gas. This Lennard-Jones parameter can be estimated for a particular material from the materials melting point, $\epsilon_A/k_B = 1.92\,T_m$. After evaluating $T^*$, Table E.1 or Eq. E2-2 in Bird et al. (2002) can be used to find the collision integral. Equation Eq. E2-2 and the evaluated terms needed to solve for the collision integral is shown here:

$$\Omega_D = \frac{1.06036}{T^{*0.15610}} + \frac{0.19300}{\exp(0.47635\,T^*)} + \frac{1.03587}{\exp(1.52996\,T^*)} + \frac{1.76474}{\exp(3.89411\,T^*)} \quad \text{(SI 2.6)}$$

**Section S3: Values and parameterizations used in this work**

Several GLY and PG vapor pressure values and parameterizations were found in literature and these are in general agreement (Stull 1947; Cammenga et al., 1977; CHERIC, 2015; Nageshwar and Mene, 1969; Curme and Johnston, 1952) and are shown in Figure S1. For compounds with unknown vapor pressure, $p_{sat}$ at some reference state and enthalpy of vaporization must be estimated to parameterize the temperature dependence.

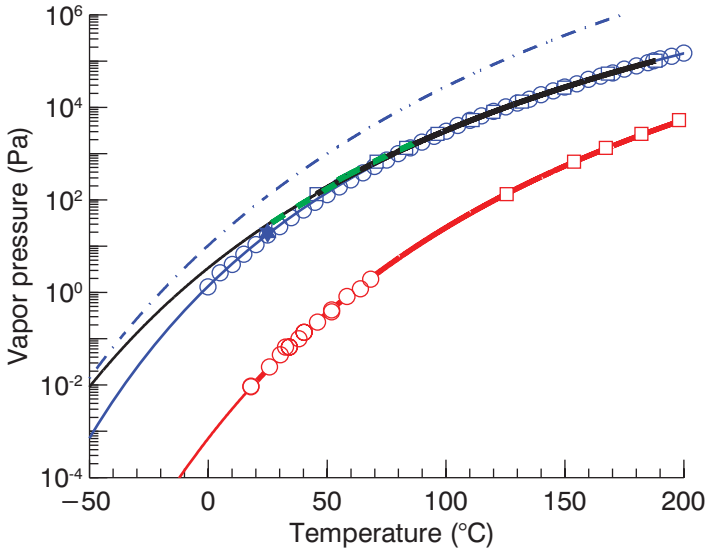


**Figure S1**: The saturation vapor pressure as a function of temperature from various literature sources for GLY (red: circle – Cammenga et al., 1977; square – Stull, 1947; solid line – CHERIC, 2015) and PG (blue: solid line – CHERIC, 2015; square – Stull, 1947; circle – Curme and Johnston, 1952; star – The Dow Chemical Co., 2003; green dashed line – Nageshwar and Mene, 1969; solid black line – NIST; blue dashed line – see text). For the black and red solid lines, thicker portions indicate the temperature ranges for which the parameterizations were reported. Thinner lines indicate extrapolation beyond the reported bounds of the parameterizations.

The literature values are in excellent agreement with each other. The PG curve that is not in agreement (blue dashed line) with the other values was a simplistic curve based on the enthalpy of vaporization (dH = 67 kJ mol$^{-1}$, NIST), a single vapor pressure measurement at standard temperature (10.4 Pa, Wolfram Alpha), and the simplified form of the Clausius-Clapeyron relationship ($p_i = A \times \exp(-\Delta H/RT)$). For this work we used the Eq. S3.1 for GLY (CHERIC, 2015) and Eq. SI 3.2 for PG (NIST) where $p_{i,sat}$ is evaluated in Pa for a given temperature in K.

$$ln(p_{i,sat}) = -21.25867ln(T) - \frac{16726.26}{T} + 165.5099 + 1.100480 \times 10^{-5}T^2 \quad \text{(SI 3.1)}$$

$$log_{10}(p_{i,sat}/10^5) = 6.07936 - \left(\frac{2692.187}{T-17.94}\right) \quad \text{(SI 3.2)}$$

It should be noted that the selected GLY vapor pressure equation was fitted to data T > 17 °C, the melting point of GLY. Values below 17 °C are extrapolated.

Using bulk humidity data for GLY and PG, the Margules fit parameters can be found. The bulk data consisted of measured $S_{H2O}$ over a flat surface and the fraction of GLY/PG versus water content present in the solution. The fraction of each component within the solution is then converted to mole fractions. Under the assumption that the water activity ($a_w$) is the same as a saturation ratio over a flat surface, the activity coefficient at each $S_{H2O}$ is $\gamma = a_w/x_w$. The resulting activity coefficient versus mol fraction data can now be fit to Eq. SI 2.4 to find the fit parameters $\alpha_m$ and $\beta_m$. Figure S2 shows the activity coefficient values derived from bulk data for GLY and PG, respectively.

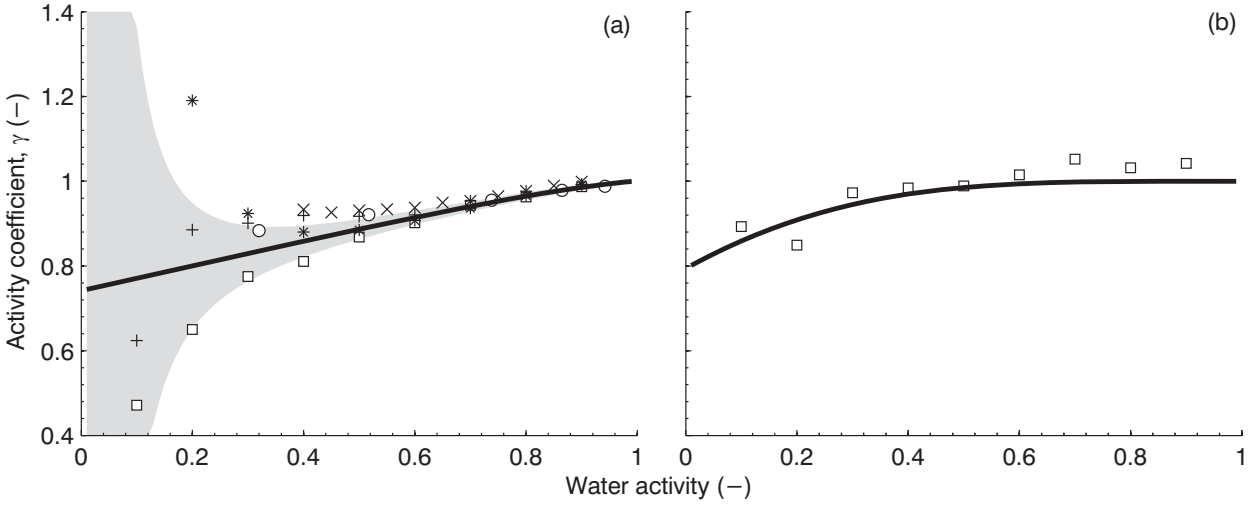


**Figure S2**: (a) GLY bulk data values. Activity coefficient data as a function of water activity. Data points are from literature (square – Glycerine Producers Association (1963); plus – The Soap and Detergent Association (1990); circle - Glycerine Producers Association (1963); star – Forney and Brandl, 1992; x – ASTM (1990)). Solid line is the Margules fit using [α, β] = [-0.2988, 1.312]. Shaded region is estimated error in activity coefficient data derived from the standard deviation of the literature data binned in 0.1 $a_w$. (b) PG bulk data values. Data points are from The Dow Chemical Co. (2003). Margules fit paraemters [α, β] = [-0.2305, 3.936]. No error region is included due to a single citation source.

## Tables

**Table 1**: Summary of parameters needed to evaluate Eq. (1), main text.

| | **Glycerol** | **Propylene glycol** | **Water** | **Air** |
|---|---|---|---|---|
| $MW$ – Molar weight/mass (g/mol) | 92.09 | 76.09 | 18.01 | 28.97 |
| $\sigma_i$ – Collision diameter (Å) | 5.333 | 5.205 | - | 3.617 |
| $\epsilon_B/k_B$ – Lennard-Jones parameter (K) | 558.62 | 411.17 | - | 97 |
| Sat. Vapor Pressure at $T$ = 20 °C (Pa) | 1.16e-2 | 19.8 | 2340 | - |
| $\sigma$ – Surface tension (N $m^{-1}$) | 0.07 | 0.04 | 0.073 | - |
| $\rho$ – Density (kg/$m^3$) | 1260 | 1040 | 1000 | - |
| $V_c$ – Critical volume ($cm^3$) | 255 | 237 | - | - |
| $T_m$ – Melting temperature (K) | 290.95 | 214.15 | - | - |
| $[\alpha_m, \beta_m]$ – Margules fit parameters | [-0.2988, 1.312] | [-0.2305, 3.936] | - | - |
| $D_i$ – Diffusivity at $T$ = 20 °C ($cm^2$ $s^{-1}$) | 0.077 | 0.086 | 0.242 | - |
| $\alpha_m$ - Mass accommodation coefficient | 0.8 | 1 | - | - |

**Section S4: Evaporation in DMA**

As the particles evaporate, the mass is transferred from the particle to the gas phase resulting in an increase in the partial pressure of that material over the surface. If the vapor pressure increases significantly this can retard particle evaporation and alter the observable kinetics of the particle. In the evaporating DMA the filter removes excess particles and vapor thus ensuring that clean air is always supplied to the DMA sheath. It is then assumed any vapor phase constituents are introduced by the sample stream and evaporation of the particles currently being classified by the DMA. As the sample stream only exists at warm temperatures for a brief period of time, the sample flow should be devoid of vapor phase material when entering the DMA (with the exception of the water vapor introduced during the humidified scans).

This leads to the question on whether a particle moving within the DMA can sufficiently out run its own vapor field. Figure S3 shows the particle motion through the DMA (blue line), the vapor field front from the initial particle evaporation when the particle is introduced into the DMA, and the relative vapor field gradient from when the particle leaves the DMA. The vapor field transits in the radial direction due to diffusion only as there is no radial motion of the sheath flow and can be modeled via: $\Delta r = 2\sqrt{D_i \Delta t}$. Conversely, the axial motion of the sheath fluid will dominate over the diffusion in the $z$ direction and is modeled as $\Delta z = Q_{sheath}\Delta t$.

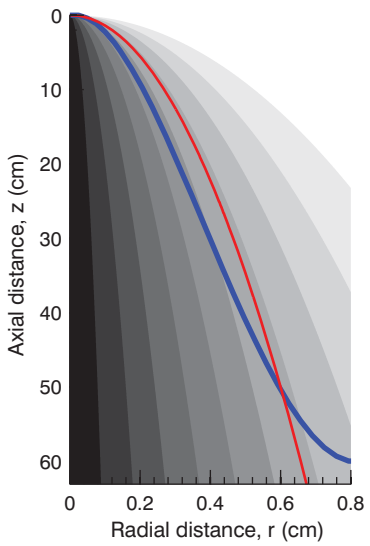


**Figure S3:** Blue line is particle trajectory within the HF-DMA. Red line is the diffusional front corresponding to the particle transit time. Gradient indicates the relative vapor concentration.

In this simplified case it can be seen that the particle resides near the vapor field front (red line) during the majority of the particle transit. Even if the GLY vapor concentration in the sample flow were high, the concentration experienced by the particle along the trajectory is substantially reduced. We note that if there was vapor buildup, this would introduce significant error and the incongruent results would have been observed at different sheath flow rates. This is because the

radial velocity leading to transmission depends on sheath flow rate, while the radial diffusion rate does not. Furthermore, we observed that the accommodation coefficient of GLY is near unity. Had vapor build-up prevented evaporation, substantially smaller $\alpha_m$ values should have been observed.

**Section S5: Hygroscopic growth parameterization**

The Margules fit parameters can be used to evaluate the equilibrium hygroscopic growth factors of pure GLY or PG particle having a dry diameter of $D_{pd}$. Detailed equations are provided in Petters et al. (2009) and Suda and Petters (2013). Figure S4 shows equilibrium hygroscopic growth factor for non-evaporating 200 nm GLY (blue) and PG (red) particles evaluated from the Margules parameterization of the bulk water activity data, molecular weight, and density provided in Table S1. The corresponding ideal hygroscopicity parameters, $\kappa_{ideal}$ (Suda and Petters, 2013), are 0.2465 and 0.2276 for GLY and PG, respectively.

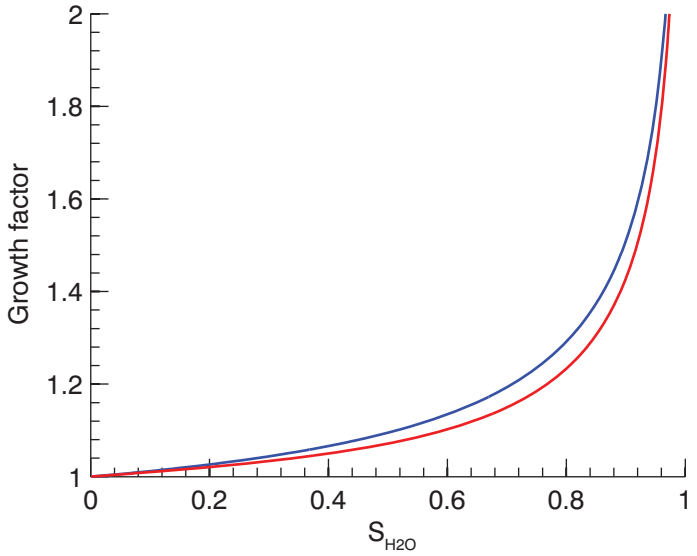


**Figure S4:** Equilibrium hygroscopic growth for GLY (blue) and PG (red).

**Section S6: Measured humidigrams**

The following eight humidigrams were used to generate the data that went into Figure 8 of the main text. Included on each humidigram is the measured growth factor (black points), equilibrium growth factor profile (black line), modeled scan results (blue line), and the same modeled results using a 10% change in the parameterized GLY vapor pressures (blue dashed lines) with increased vapor pressure model results appearing below the standard modeled results.

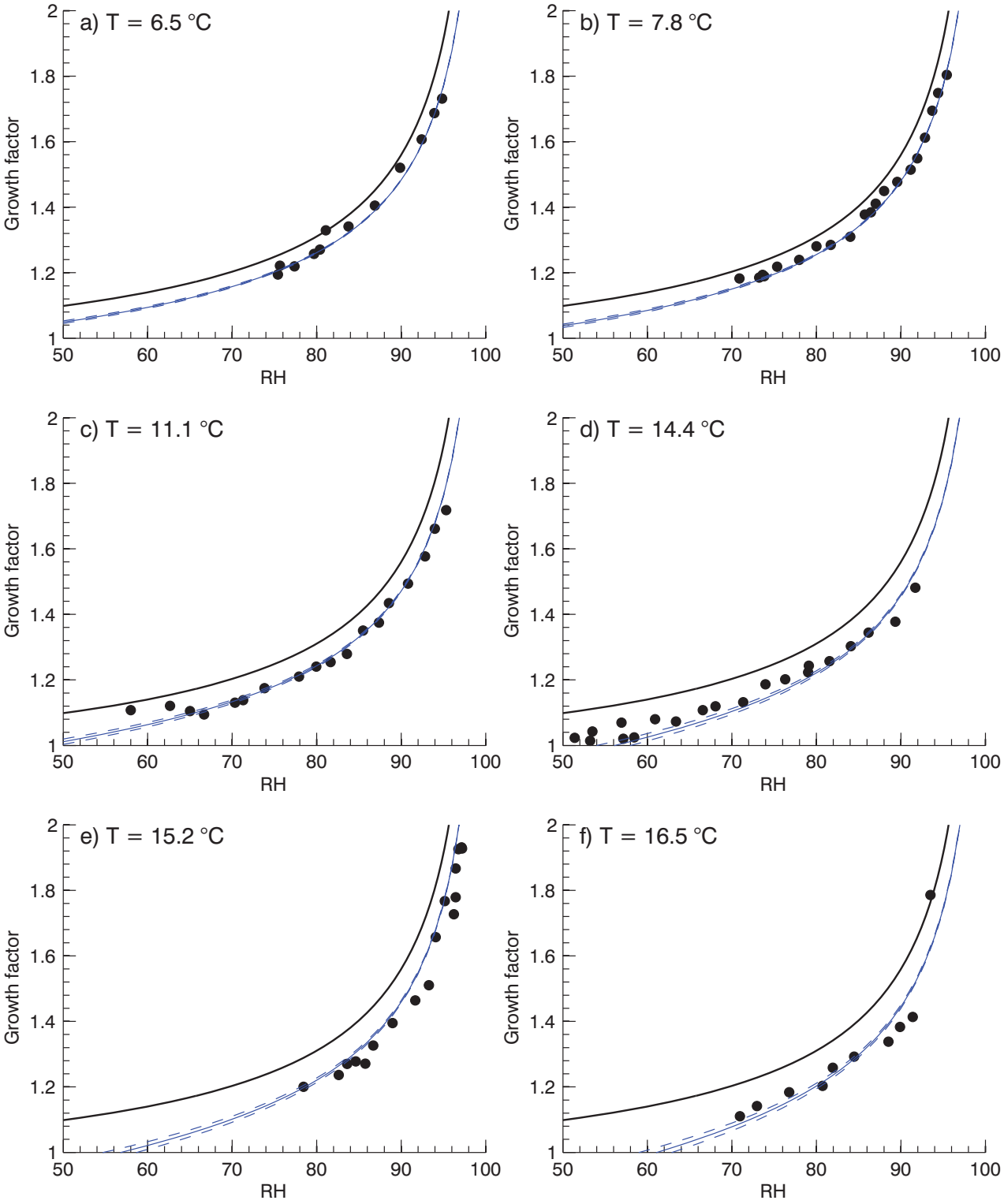
a) T = 6.5 °C
b) T = 7.8 °C
c) T = 11.1 °C
d) T = 14.4 °C
e) T = 15.2 °C
f) T = 16.5 °C
Growth factor
RH
1
1.2
1.4
1.6
1.8
2
50
60
70
80
90
100

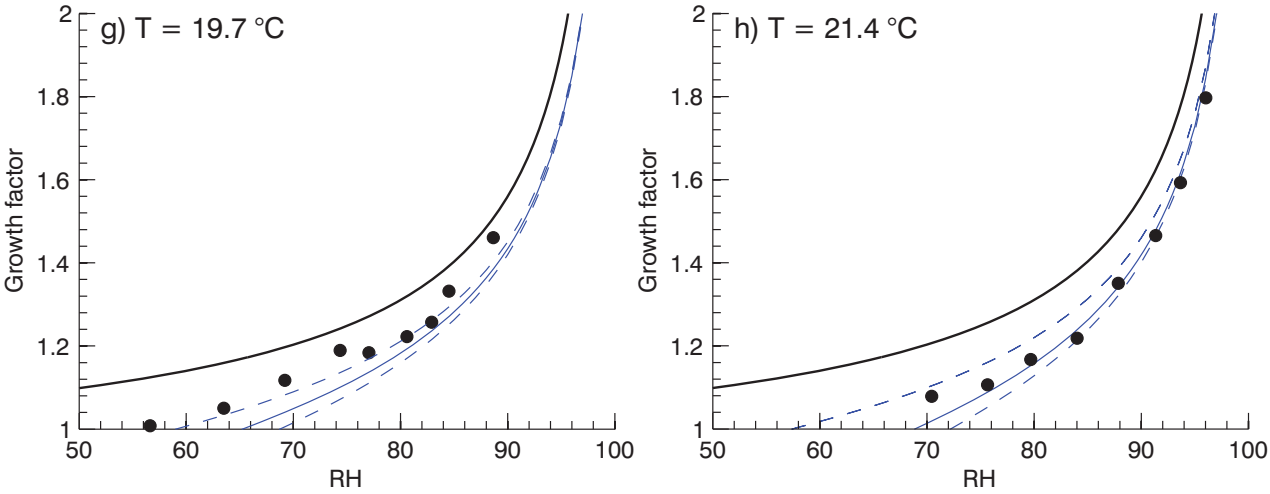
g) T = 19.7 °C
h) T = 21.4 °C
Growth factor
RH
2
1.8
1.6
1.4
1.2
1
50
60
70
80
90
100

**References**


ASTM International (1990), ASTM Standard D5032, "Standard Practice for Maintaining Constant Relative Humidity by Means of Aqueous Glycerin Solutions," , doi:10.1520/D5032-11.

Bilde, M., B. Svenningsson, J. Mønster, and T. Rosenørn (2003), Even−Odd Alternation of Evaporation Rates and Vapor Pressures of C3−C9 Dicarboxylic Acid Aerosols, *Environ. Sci. Technol.*, *37*(7), 1371–1378, doi:10.1021/es0201810.

Bird, R. B., W. E. Stewart, and E. N. Lightfoot (2002), *Transport phenomena*, 2nd ed., John Wiley & Sons, Inc., New York.

Cammenga, H. K., F. W. Schulze, and W. Theuerl (1977), Vapor pressure and evaporation coefficient of glycerol, *J. Chem. Eng. Data*, *22*(2), 131–134, doi:10.1021/je60073a004.

Curme, and Johnston (1952), *Glycols*, Reinhold Publishing Corp., New York.

Forney, C. F., and D. G. Brandl (1992), Control of humidity in small controlled environment chambers using glycerol-water solutions, *Horttechnology*, *2*(1), 52–54.

Fuchs, N. A., and A. G. Sutugin (1971), High-dispersed Aerosols, in *Topics in Current Aerosol Research*, p. 1, Elsevier.

Glycerine Producers Association (1963), *Physical properties of glycerine and its solutions*, Glycerine Producers' Association, New York, NY.

Knutson, E. O., and K. T. Whitby (1975), Aerosol classification by electric mobility: apparatus, theory, and applications, *J. Aerosol Sci.*, *6*(6), 443–451, doi:10.1016/0021-8502(75)90060-9.

Linstrom, P. J., and E. Mallard, W. G. (2015), *NIST Chemistry WebBook, NIST Standard Reference Database Number 69*, National Institute of Standards and Technology, Gaithersburg, MD.

Lydersen, A. L., R. A. Greenkorn, and O. A. Hougen (1955), *Estimation of Critical Properties of Organic Compounds by the Method of Group Contribuitons*, Engineering Experiment Station Report 3, University of Wisconsin College of Engineering, Madison.

Nageshwar, G. D., and P. S. Mene (2007), Vapour-liquid equilibrium data for n-butyl acetate-1,2-propylene glycol, *J. Appl. Chem.*, *19*(7), 195–196, doi:10.1002/jctb.5010190704.

Petters, M. D., H. Wex, C. M. Carrico, E. Hallbauer, A. Massling, G. R. McMeeking, L. Poulain, Z. Wu, S. M. Kreidenweis, and F. Stratmann (2009), Towards closing the gap between hygroscopic growth and activation for secondary organic aerosol – Part 2: Theoretical approaches, *Atmos. Chem. Phys.*, *9*(12), 3999–4009, doi:10.5194/acp-9-3999-2009.

Prausnitz, J. M., R. N. Lichtenthaler, and E. G. Azevedo (1999), *Molecular thermodynamics of fluid-phase equilibria*, Prentice Hall PTR, Upper Saddle River, NJ.

Suda, S. R., and M. D. Petters (2013), Accurate Determination of Aerosol Activity Coefficients at Relative Humidities up to 99% Using the Hygroscopicity Tandem Differential Mobility Analyzer Technique, *Aerosol Sci. Technol.*, *47*(9), 991–1000, doi:10.1080/02786826.2013.807906.

Stull, D. R. (1947), Vapor Pressure of Pure Substances. Organic and Inorganic Compounds, *Ind. Eng. Chem.*, *39*(4), 517–540, doi:10.1021/ie50448a022.

The Dow Chemical Co. (2003), *A guide to glycols*, Midland, MI.

The Soap and Detergent Association (1990), *Glycerine: an overview*, The Soap and Detergent Association: Glycerine & Oleochemical Division, New York, NY.

Wilkes, J. O. (2005), *Fluid Mechanics for Chemical Engineers with Microfluidics and CFD*, 2nd ed., Prentice Hall, Upper Saddle River, New Jersey.